

to appear in ApJ 20 December 2004, v617

An *XMM-Newton* Observation of the Seyfert 2 Galaxy NGC 6300. I. The Nucleus

Chiho Matsumoto¹, Aida Nava, Larry A. Maddox, Karen M. Leighly

Department of Physics and Astronomy, The University of Oklahoma, 440 West Brooks Street, Norman, OK 73019

Dirk Grupe

Astronomy Department, The Ohio State University, 140 West 18th Avenue, Columbus, OH 43210

Hisamitsu Awaki

Department of Physics, Faculty of Science, Ehime University, Bunkyo-cho, Matsuyama, Ehime 790-8577, Japan

and

Shiro Ueno

Institute of Space and Astronautical Science, Japan Aerospace Exploration Agency, 2-1-1 Sengen, Tsukuba, Ibaraki 305-8505, Japan

ABSTRACT

We present results from a half-day observation by *XMM-Newton* of the nucleus of the nearby Seyfert 2 galaxy NGC 6300. The X-ray spectrum of the nucleus consists of a heavily absorbed hard component dominating the 3–10 keV band and a soft component seen in the 0.2–2 keV band. In the hard band, the spectrum is well fitted by a power-law model with photon index of 1.83 ± 0.08 attenuated by a Compton-thin absorber ($N_{\text{H}} \simeq 2.2 \times 10^{23} \text{ cm}^{-2}$). A narrow iron line is detected at $6.43^{+0.01}_{-0.02}$ keV with an equivalent width of ~ 150 eV; the line velocity width is marginally resolved to be $\sigma \sim 60$ eV. The soft emission can be modeled as

¹Current address: EcoTopia Science Institute, Nagoya University, Furo-cho, Chikusa, Nagoya, 464-8603, Japan; Email: chiho@u.phys.nagoya-u.ac.jp

a power-law and may be emission scattered by surrounding plasma. Rapid and high-amplitude variability is observed in the hard X-ray band, whereas both the iron line and the soft emission show no significant variability. It is suggested that the nucleus has experienced an overall long-term trend of decreasing hard X-ray intensity on a timescale of years. We discuss the origins of the spectral components.

Subject headings: galaxies: Seyfert, galaxies: X-ray, individual: NGC 6300

1. Introduction

NGC 6300 is a nearby ($z=0.0037$; Mathewson & Ford 1996) ringed, barred spiral galaxy, classified as a SB(rs)b from its morphology, and also identified as a bright Seyfert 2 from spectroscopy. It was first detected in hard X-rays in 1991 February during a *Ginga* maneuver (Awaki 1991). Then, it was observed in the 3–24 keV band by *RXTE* in 1997 February, and in the 0.1–200 keV band by *Beppo-SAX* in 1999 August. *RXTE* measured a flat continuum spectrum (photon index: $\Gamma \simeq 0.68$) with a superimposed K- α neutral iron emission line of large equivalent width ($EW \simeq 470$ eV). These spectral properties imply the presence of a Compton thick absorber obscuring the nucleus (Leighly et al. 1999). Two-and-a-half years later, *Beppo-SAX* obtained a spectrum that was brighter in the whole 3–20 keV band, seen through a Compton thin absorber ($N_H \simeq 2.1\text{--}3.1 \times 10^{23} \text{ cm}^{-2}$), but with an iron line of the same intensity as the *RXTE* line (Guainazzi 2002). The spectral differences between the two observations are most likely associated with the transient behavior of the Seyfert nucleus, which was probably caught in a high activity stage during the *Beppo-SAX* observation (Guainazzi 2002). NGC 6300 is one of a few known objects exhibiting transitions between Compton-thin and Compton-thick X-ray spectral states (Matt et al. 2003).

In this paper we present the results from a new observation of NGC 6300 with *XMM-Newton* (Jansen et al. 2001), focusing on the spectral properties and the resulting physical view of the nucleus. Preliminary results have been presented by Nava et al. (2003) and Maddox et al. (2002). Section 2 describes the observation and the data preparation, in §3 we perform image analyses in the soft and hard X-ray bands, and in §4 we examine variability in some energy bands. Using the results from §3 and §4, we perform a spectral analysis. Finally, we discuss the physical conditions of the spectral components and speculate on their origins.

Throughout this paper error bars in figures are 1σ , and uncertainties quoted in the body and tables are 90% confidence for one parameter of interest.

2. Observation and Data Preparation

NGC 6300 was observed from 2001 March 2 3:35 to 16:36 (UT) with *XMM-Newton*. The EPIC instruments consisting of one pn (Strüder et al. 2001) and two MOS (Turner et al. 2001) CCDs were operated in full-frame imaging mode using the medium filter. The background during the whole observation was low so that the entire observation could be used. We did not analyze the Reflection Grating Spectrometer (RGS; den Herder et al., 2001) data because of the low number of photons.

The data could not be reduced in the standard way because the observation was split into two observation IDs (ObsIDs), 0059770101 between 03:35–05:32 and 0059770201 between 05:43–16:34. The first ObsID contained the pn and MOS data, while the second contained the RGS and Optical Monitor (OM) data. However, while the event files in these ObsIDs were complete, the housekeeping data only contained the times given above for the ObsIDs. Therefore, the housekeeping data had to be merged. We merge the files using the FTOOLS task `fmerge` as described on the MPE Cookbook page.¹ After this procedure the EPIC event lists were created in the standard way using the Science Analysis Software (SAS) version 5.3.0. We filtered further using HEAsoft versions 5.1 and 5.2. We used SAS version 5.3.3 to create the response matrices.² Throughout we used the “flag=0” events with the pattern of 0–4 and 0–12 from the pn and MOS detectors, respectively.

3. Image Analysis

Figure 1 shows the X-ray contour plots in the soft and hard X-ray bands. In the hard X-ray image, the primary source is located at R.A.= $17^{\text{h}} 16^{\text{m}} 59.8^{\text{s}}$ and decl.= $-62^{\circ} 49' 13''$ (J2000.0), which is consistent with the position of the radio (13 cm) core emission.³ In the soft band, a point-like source is detected at the position of the primary hard X-ray source. At least two more point-like sources are detected within $80''$ separation from the nucleus, and emission from the host galaxy is also detected around the nucleus. One of the point sources may be a new candidate ultra-luminous X-ray source. Since the origin of these emissions is difficult to determine solely from the X-ray observation, details of the

¹ Available at http://wave.xray.mpe.mpg.de/xmm/cookbook/EPIC.PN/merge_odf.html.

²We had used the latest version when the analysis was done. To check consistency with the newer calibration, we reduced the data and created response matrices using the latest SAS version 5.4.1. The parameters of our final model in Table 3 were consistent with those from SAS 5.4.1.

³R.A.= $17^{\text{h}} 16^{\text{m}} 59.6^{\text{s}}$, decl.= $-62^{\circ} 49' 16''$ with the beam size of $\sigma \sim 4''$ (Maddox et al., in prep.)

point-source properties and galaxy emission will be presented in a separate paper involving analysis of multi-wavelength observations (Maddox et al., in preparation).

We made a radial profile of the nucleus, in order to investigate whether or not the nuclear emission is a point source. Figure 2 shows the radial profile from the MOS detectors in the soft and hard bands. The radial profile in the hard band is described well by the point-spread function (PSF) model (Ghizzardi 2001) plus constant offset, which represents the background. Thus, we conclude that the hard emission cannot be distinguished from a point source. However, as suggested by the image, the soft radial profile cannot be expressed solely by the PSF model for a point source. We fitted the data with the King and constant models in the regions of $r < 10''$ and $r > 150''$, respectively. In this fit, parameters of the King model other than the normalization were fixed at the values for a point source given by Ghizzardi (2001). Although the radial profile shows an apparent excess at $r \sim 20\text{--}70''$ that is apparently due to emission in the galaxy, the core of the observed PSF within $r \lesssim 16''$ is consistent with being a point source, and therefore the nuclear emission is unresolved.

4. Time Series Analysis

Figure 3 shows the pn light curves in the soft (0.2–2 keV) and hard (2–10 keV) bands. In the hard band, rapid and rather high amplitude variability is clearly seen, whereas the light curve is consistent with constant in the soft band ($\chi^2 = 23.5$ for 25 degrees of freedom [dof]).

To search for spectral variability, we computed the fractional excess variance as a function of energy (Figure 4). Around 2 keV the variance is low; this can be explained by dilution of the varying hard component by the less-variable soft emission. The larger variance around 4 keV may imply that the spectrum is softer when it is brighter. The variability drops around 6.4 keV, indicating a less-variable iron line. These points are investigated further in §5.1.

5. Spectral Analysis

Because of the differences in the radial profiles, we performed spectral analysis separately in two energy bands. For the hard-band analysis, we extracted the spectra from a circular region with $r < 60''$. The background spectra were collected from a source-free region near the nuclear-spectra-extracted region. For the soft X-ray analysis, we extracted spectra from $r < 16''$ regions, to avoid contamination from the surrounding galaxy emission. Each spectrum is grouped so that each energy bin has at least 25 photons and so that the energy

bin widths are about half the detector resolution ($\sigma \sim 35\text{--}70$ eV). The response matrices were created using `rmfgen` and `arfgen` in SAS 5.3.3. The χ^2 fitting statistics were used.

5.1. Hard X-ray Spectrum

The hard X-ray spectrum of the nucleus peaks at around 5 keV (Figure 5), and it is apparent that intervening column density is larger than the Galactic column density of 9.38×10^{20} cm $^{-2}$ (Dickey & Lockman 1990). Thus, we fitted the 3–10 keV data with a model of a power-law attenuated by Galactic and intrinsic absorption. The background flux is only a few percent of the source flux in the hard band. As a result of a prominent emission line at ~ 6 keV, the presence of which has been suggested by Figure 4, the fits are not acceptable for any EPIC spectra ($\chi^2_\nu = 1.96$, 1.41, and 1.30 for 234, 156, and 155 dof for the pn, MOS1, and MOS2, respectively). Therefore, we added a Gaussian to the model to represent the line, and the fits are improved significantly. The results are listed in Table 1; the parameters are consistent among the three detectors. The fits are statistically acceptable for both of the MOS spectra; for the pn spectrum, the fit is not acceptable at 90% confidence level, however it is not rejected at the 99.6% confidence level and would be acceptable at 90% if there were a 4% uncertainty in the calibration.

Next, we performed a simultaneous fit of pn and MOS1+2 spectra with this model and found that the 3–10 keV spectra are well reproduced with a rather typical model for Compton-thin Seyfert 2 galaxies: an absorbed power-law and a relatively narrow iron line (Figure 5). The photon index (Γ) is 1.83 ± 0.08 , and the intrinsic column density (N_{H}) is $\sim 2.2 \times 10^{23}$ cm $^{-2}$. The absorption-corrected 2–10 keV luminosity is 1.3×10^{42} erg s $^{-1}$, assuming $H_0 = 50$ km s $^{-1}$ Mpc $^{-1}$.⁴ For the line, we obtained the central energy of $6.43^{+0.01}_{-0.02}$ keV, indicating that the iron is not significantly ionized. The line width σ is marginally resolved to be 55^{+19}_{-21} eV. If we assume that the line is also attenuated by the intrinsic absorber, the equivalent width (EW) of the iron line is 148 ± 18 eV.

We also made spectral fits to time-resolved spectra in order to confirm the suggested variability behavior of each spectral component discussed in §4. The light curve was split into five segments such that each segment corresponds to a particular state of the flux (i.e., high, low, decreasing, etc.) and so that the duration of each segment is approximately equal to 1×10^4 s (Figure 3). We fitted the resulting five sets of spectra in the same manner as described in the previous paragraph. The soft spectra were not examined because the photon statistics are poor and because the light-curve analysis revealed no significant variability in

⁴The luminosity is 6.2×10^{41} ergs s $^{-1}$ using the *WMAP* cosmological parameter of $H_0 = 72$ km s $^{-1}$ Mpc $^{-1}$.

the soft band. We performed model fits in which all parameters were allowed to vary; we found significant variability in only the power-law normalization. It is noteworthy that the intensity of the iron line remains constant, despite the factor of 2.6 variation of the ionizing continuum flux. If the iron line would have instantaneously responded to the continuum, its variability should have been clearly detected above the rather small statistical uncertainties on the iron line intensity ($\sim 15\%$).

The reflection component, which is characterized by a hump around 20 keV, has been intensively studied using the previous observations that were made by satellites with good efficiency above 20 keV. In the *XMM-Newton* bandpass, which extends to ~ 10 keV only, the reflection component is not prominent; thus, the data are not very sensitive to the reflection model. Therefore, we investigated this model holding some spectral parameters fixed. We made fits using a reflection model from a neutral disk (`pexrav`), assuming that the incident photons on the disk have a power-law spectrum with the observed power-law index and that the abundances of the disk are solar. We tested the cases in which the cut-off energy of the power-law is 100 or 250 keV and the absorption column density for the reflection component is only Galactic or is the same as the nucleus. The choice of the assumed values did not affect the result of the fit significantly; addition of the reflection improved the fits by $\Delta\chi^2 \sim 7\text{--}10$, and the photon index became slightly steeper ($\Delta\Gamma \sim 0.10$). The parameters of the iron line were not significantly affected. The contribution of the reflection component is 12%–17% of the total model flux in the 3–10 keV band; in terms of the reflection parameter R ,⁵ the flux is equivalent to $R = 1.3_{-0.9}^{+1.1}$, $1.7_{-1.1}^{+1.4}$, and $4.8_{-3.1}^{+3.8}$, assuming that we observe through an absorption with the same column density as that of the nucleus at the inclination angle⁶ of 30° , 60° , and 85° , respectively.

5.2. Soft X-ray Spectrum

5.2.1. Background

The background (BGD) subtraction is a difficult issue for the soft X-ray analysis because the soft emission from the active galactic nucleus (AGN) is faint and because it is not known a priori whether the soft X-ray emission from the host galaxy extends close to the AGN. Thus, we considered two BGD spectra sets.

Assuming that the host galaxy emission is confined to the galactic ring and does not

⁵ $R = 1$ corresponds to an illuminated solid angle of 2π for isotropic incident emission.

⁶These angles are measured from axis of symmetry.

contaminate the nuclear spectrum, we extracted one set of BGD spectra (BGD1) from the source-free-region at the distance $r > 2'$. We also considered the complementary assumption, that the soft X-ray emission from the galaxy is approximately uniform through the region. For this, another set (BGD2) is collected from the region where extended emission is prominent, including a rectangular region ($70'' \times 40''$; shown in Figure 1) and excluding the region of $r < 20''$ from the nucleus. In general, using BGD2 results in somewhat flatter spectral shape (e.g., $\Delta\Gamma \sim 0.3$) and $\sim 35\%$ reduction in flux.

5.2.2. Absorption of the Reprocessed Emission

Another difficulty in the soft X-ray spectral analysis is the question of the magnitude of the absorption of the reflection component. If the reflection is attenuated by the same absorption as the nucleus, the emission is negligible below about 2 keV. However, since NGC 6300 was seen with *RXTE* to be reflection-dominated, the reflection may not be attenuated by the same absorption as the nucleus. In this case, reflection can dominate in the 1–3 keV band.

In order to estimate the magnitude of the absorption for the reprocessed emission, we fitted the 2–10 keV data assuming that the reprocessed emission is covered by an absorption column density $N_{\text{H}repr}$, which is left free in the fit. Although the fit could not constrain $N_{\text{H}repr}$ owing to limited data quality, the best-fit value was $\sim 2 \times 10^{22} \text{ cm}^{-2}$, regardless of the assumed reflection parameters and the choice of the background. If $N_{\text{H}repr} \sim 2 \times 10^{22} \text{ cm}^{-2}$, then the reflection component is insignificant below 1.6 keV.

5.2.3. Spectral Modeling

With the absorption estimated in the previous section, we performed the following fits in the 0.2–1.6 keV band.

First, we modeled the soft spectra with a Galactic absorbed power-law and obtained acceptable χ^2_ν values (0.92 and 0.62 for 35 dof with BGD1 and BGD2, respectively). The spectra and the best-fit model with BGD1 are shown in Figure 6, and the parameters are summarized in Table 2. The soft photon index (Γ_{soft}) is $2.00^{+0.16}_{-0.18}$ and $1.72^{+0.26}_{-0.28}$ using BGD1 and BGD2, respectively. These values are consistent with the hard photon index ($\Gamma_{\text{hard}} = 1.83 \pm 0.08$), suggesting that the soft emission could be nuclear continuum scattered by electrons. The ratio of the soft to hard power-law flux is 0.2%–0.3% in the 0.2–2.0 keV band.

It is also possible that the soft X-ray emission originates in optically-thin hot gas associ-

ated with possible starburst activity. The Raymond-Smith thermal plasma model in XSPEC was used to test this scenario. The fit results are also listed in Table 2. This model is not rejected statistically, and the size of the plasma⁷ deduced from the X-ray intensity can be consistent with the radial profile of the X-ray image. However, the obtained abundance was small: the 90% upper limit is 0.01 and 0.1 solar for BGD1 and BGD2, respectively. With BGD1, this model was rejected at the 99% confidence level in the abundance regime larger than 0.3 solar. Although we cannot rule out this model, this model is not preferred because of the very low abundances.

Finally, we considered intrinsic absorption for the soft X-ray emission from the nucleus, by adding an additional absorption component in the above models. The fit results are also summarized in Table 2. In most cases, intrinsic absorption is not statistically required. Only the power-law model fit with BGD1 improved (96% by the *F*-test); however, the 90% lower-limit of N_{H} is as small as $1 \times 10^{20} \text{ cm}^{-2}$. In every fit, the upper-limit of N_{H} is $1 - 2 \times 10^{21} \text{ cm}^{-2}$. This result suggests that the soft X-ray-emitting region is not covered by a significant amount of absorbing gas intrinsic to NGC 6300.

5.3. Overall Picture

Finally, we fitted the data in the entire *XMM-Newton* bandpass. The model included all spectral components that have been considered before. Specifically, the spectral model consists of (1) a hard power-law attenuated by an intrinsic absorption of $N_{\text{H}hard}$, (2) reprocessed emission attenuated by another intrinsic absorber of $N_{\text{H}repr}$, and (3) a soft power-law without intrinsic absorption. Assuming that the soft X-ray emission is electron-scattered nuclear power-law emission and self-absorption is negligible, the soft power-law index is constrained to be the same as the hard power-law index. All components are attenuated by Galactic absorption. The best-fit spectral model is shown in Figure 7, and the parameters are summarized in Table 3. This model can reproduce the observed spectrum in the whole band ($\chi^2_{\nu} = 0.92$ for 475 dof).

⁷Assuming that the plasma is uniform in density, n (cm^{-3}), the size of the plasma is estimated to be $\sim 10^2 (1/n)^{-2/3} \text{ pc}$.

6. Discussion

6.1. On the Origin of the Soft X-ray Emission

The *XMM-Newton* observation allowed us to investigate the nuclear spectrum of NGC 6300 for the first time without contamination from the surrounding emission. We found that it can be modeled with a power-law having the same photon index as that in the hard band. One possible origin for this emission would be that the soft X-rays are nuclear emission leaking through an inhomogeneous absorber. However, this model is rejected by the smaller variability amplitude in the soft band. Thus, the soft emission can be considered to be nuclear emission scattered by electrons with some spatial extent that serves to smear out the variability of incident nuclear emission.

Recent high-resolution spectra have revealed that soft X-ray emission in some Seyfert 2 galaxies originates from photoionized plasma (e.g., Sako et al. 2000; Sambruna et al. 2001). Unfortunately NGC 6300 is not bright enough to investigate with the RGS; however, the EPIC spectra suggest the presence of some emission line-like features at about 0.8 and 1.9 keV (see the bottom panel of Figure 6). If we add a narrow ($\sigma = 0$) Gaussian to the final model (Table 3), the fits improved at the 99% and 92% confidence levels (by the *F*-test) with the line at $0.84^{+0.09}_{-0.04}$ and $1.90^{+0.07}_{-0.12}$ keV, respectively. These energies suggest that if they are emission lines, they may be Fe L- and/or Ne K-lines, as well as Si K-lines; if they are radiative recombination continua (RRCs), they may be those from O and Mg ions. Regardless of whether they are lines and/or RRCs, the observed energies suggest that the ions are highly ionized. Thus, the plasma should be rich with free electrons, and the emission scattered by the electrons can also contribute to the soft X-ray emission. Actually, the observed soft spectrum is so smooth that it cannot be described solely by a model of a photoionized plasma emission calculated by `xstar2xspec`⁸ because the model predicts more prominent line features if abundance is about solar. In reality, both components are likely to contribute to the soft X-ray emission; however, because of the limited data quality, it is impossible to investigate further.

6.2. Long-Term Variability and Comparison with the Previous Observations

6.2.1. Soft X-ray

XMM-Newton observed that the 0.2–2 keV flux from the nucleus is $3\text{--}4 \times 10^{-14}$ erg cm $^{-2}$ s $^{-1}$

⁸See <http://heasarc.gsfc.nasa.gov/docs/software/lheasoft/xstar/xstar.html>.

without correcting for Galactic absorption. Below we compare this value with the previous values from other instruments.

In 1979, NGC 6300 was observed by the *Einstein* IPC (spatial resolution of $\sim 1''$), and the 3σ upper limit to the count rate was 1.19×10^{-2} counts s^{-1} between 0.2 and 4.0 keV (Fabbiano, Kim & Trinchieri 1992). This count rate corresponds to the upper limit of the absorption-uncorrected 0.2–2 keV flux of $2\text{--}4 \times 10^{-13}$ ergs $cm^{-2} s^{-1}$, using the Galactic absorbed power-law model with Γ in the range of 1–5.

ROSAT made three observations of NGC 6300 with the HRI (half power radius is about $4''$) and detected the object twice.⁹ The count rates were $(3.9 \pm 1.3) \times 10^{-3}$ counts s^{-1} in 1997 October and $(1.1 \pm 0.5) \times 10^{-3}$ counts s^{-1} in 1998 March.¹⁰ Although the flux might have decreased between two observations, the significance of that inference is low. We converted the weighted mean count rate of 1.5×10^{-3} counts s^{-1} into flux using the Galactic absorbed power-law model with Γ in the range of 1–5; the count rate corresponds to the absorption uncorrected 0.2–2 keV flux of $5\text{--}6 \times 10^{-14}$ erg $cm^{-2} s^{-1}$.

The *Beppo-SAX* LECS (half-power radius is 3.5 arcmin at 0.25 keV) observed in 1999 that the 0.1–2 keV count rate is ~ 0.01 counts s^{-1} integrated over the $r < 8'$ region from the nucleus (Guainazzi 2002). For the best-fit power-law model (Galactic absorbed power-law with $\Gamma \simeq 4.5$), the LECS count rate corresponds to the 0.2–2 keV flux of $\sim 1 \times 10^{-12}$ ergs $cm^{-2} s^{-1}$ uncorrected for Galactic absorption. However, the integration area is pretty large because of the *Beppo-SAX* spatial resolution. If we look at the 0.2–2 keV *XMM-Newton* image, we can see that there were a handful of point-like sources and “diffuse” galaxy emission in the $r < 8'$ region. The fraction of the count rate of the nucleus was about 10% among the total count rate from the $r < 8'$ region. Although the fraction can be time-variable, the *Beppo-SAX* flux should be heavily contaminated with surrounding emissions. Thus, we regard the soft flux from the *Beppo-SAX* observation as an upper-limit.

The observed *XMM-Newton* 0.2–2 keV flux of $3\text{--}4 \times 10^{-14}$ ergs $cm^{-2} s^{-1}$ is consistent with the *ROSAT* flux taking into account the uncertainties, and is smaller than the upper-limit from the *Einstein* and *Beppo-SAX* observations. Thus, the soft X-ray flux is consistent with being non-variable on long time scales, and this result is consistent with a view that the soft X-ray emission results from plasma with large spatial extent.

⁹The target was not detected in the shortest observation, which had an exposure of only 1 ks.

¹⁰From “ROSAT Source Browser” at <http://www.xray.mpe.mpg.de/cgi-bin/rosat/src-browser>.

6.2.2. Hard X-ray Continuum

Before this *XMM-Newton* observation, *RXTE* and *Beppo-SAX* had performed hard X-ray observations of NGC 6300. In the hard X-ray band the nuclear emission is dominant and is brighter than the second-brightest source in the *XMM-Newton* field by ~ 2 orders of magnitude. Thus, the results from *RXTE* and *Beppo-SAX* are considered to be free of contamination from serendipitous emission.

The hard X-ray fluxes from the multiple missions are summarized in Table 4. The observed 2–10 keV flux from this *XMM-Newton* observation is 8.6×10^{-12} ergs cm $^{-2}$ s $^{-1}$, which is between the *Beppo-SAX* flux of 1.3×10^{-11} ergs cm $^{-2}$ s $^{-1}$ and the *RXTE* flux of 6.4×10^{-12} ergs cm $^{-2}$ s $^{-1}$. The column density of the Compton-thin absorber of the hard power-law is consistent with a constant between the *XMM-Newton* and *Beppo-SAX* observations.

The high ratio of the *RXTE* flux to the *XMM-Newton* flux (74%) indicates that the bright reflection component seen by *RXTE* was not present during the *XMM-Newton* observation. In fact, the *RXTE* Compton reflection model predicts higher flux in the 1–3 keV energy band than was observed in the *XMM-Newton* spectra. In order to suppress the model-predicted flux so that it is smaller than the observed one using neutral absorption, a column density larger than 5×10^{22} cm $^{-2}$ is required. If such absorption were present, the *RXTE* flux from reflection in the 2–10 keV band would be 5.1×10^{-12} erg cm $^{-2}$ s $^{-1}$, which would still comprise 60% of the observed *XMM-Newton* 2–10 keV flux. Can the *XMM-Newton* spectrum accommodate such large reflection? To test this idea, we fitted the 2–10 keV *XMM-Newton* spectra with a model consisting of this reflection, an absorbed power-law, and an iron line. This fit yields $\Gamma = 2.6 \pm 0.2$, which is notably steep among Seyfert 1 and 2 galaxies. If we allow the normalization to vary while retaining the shape of the reflection component, we find that the normalization of the reflection should be only 26_{-15}^{+25} % of that observed by *RXTE*. Thus, it seems that the flux of the reflection component has decreased over the 4 yr spanned by the *RXTE* and *XMM-Newton* observations. Since these observations are separated by 4 yr, such long-timescale variability would be consistent with reflection from the putative torus, which is considered to be located at about 1 pc from the central engine.

Guainazzi (2002) has already reported that the Compton reprocessing matter should be located within $\simeq 0.75$ pc based on the large value of the relative Compton-reflection flux ($R = 4.2_{-1.7}^{+2.6}$) measured during the *Beppo-SAX* observation. He argues that it can be explained by considering that (1) the AGN was switched off during the *RXTE* observation, (2) it was switched on between the *RXTE* and *Beppo-SAX* observations and was brighter than during the *Beppo-SAX* observation, and (3) the reprocessed emission during the *Beppo-SAX* observation was echoing the past glorious state. However, if the uncertainties are taken

into account, the change of the reprocessed continuum flux between *RXTE* and *Beppo-SAX* observations is statistically marginal.¹¹ Thus, considering only the *RXTE* and *Beppo-SAX* results, we cannot distinguish between the possibilities that the reprocessing material is located farther away from the central source and that the reflection component remains constant. We infer from the *XMM-Newton* observation that a significant reduction in the reprocessed flux has occurred, so we can now rule out the possibility that the reflection flux is constant.

6.2.3. Iron Emission Line

The intensity of the iron emission line from *XMM-Newton* shows significant reduction in flux, compared with that from *RXTE* (Table 4). The intensity inferred from the *Beppo-SAX* spectrum is between those obtained from the *RXTE* and *XMM-Newton* spectra, although the *Beppo-SAX* value is consistent with either of the *RXTE* and *XMM-Newton* values, within the uncertainties. Since the iron-line flux and the reflection flux are considered to be time-averaged echoes of nuclear emission, the observed trend of decreasing reprocessed flux suggests that the nucleus has experienced an overall long-term trend of decreasing intensity on a timescale of years.

It should be noted that the EW of the iron line with respect to the reflection continuum is consistent with being constant among the three observations. This constancy is expected, if the iron line and reflection originate in the same gas and hence reflect the past nuclear activity at the same period.

The iron-line EW with respect to the reflection continuum was found to be 400–500 eV, combining the results from the three hard X-ray observations. The EW with respect to the reflection continuum is determined by geometry and abundance. For a disk geometry, it is calculated to be 1–2 keV (depending on the inclination angle; solar abundance is assumed; Matt et al., 1991). The observed EW is smaller than the theoretical expectation assuming solar abundance of iron. For a torus geometry, the predicted EW is also about 1 keV (e.g., Figure 3 of Matt et al., 2003), and thus the observed EW is again somewhat smaller. This result may suggest that iron abundance is subsolar, as has already been pointed out by Leighly et al. (1999).

¹¹By comparing the fluxes at 20 keV of Figure 5 in his paper, the variation should be less than a factor of 2. Even at 20 keV, the power-law flux still contributes \sim 25% of the total flux in the *Beppo-SAX* spectrum. The uncertainty of reflection normalization R is as large as \sim 50% according to his Table 1.

6.3. On the Origin of the Iron Emission Line

The *XMM-Newton* observation allowed us to examine the iron K- α emission line with sufficient energy resolution to distinguish its ionization level. We found from the line energy that the iron is not significantly ionized. The line width is marginally resolved to be $\sigma \sim 55^{+19}_{-21}$ eV; the detector resolution is $\sigma \sim 60$ eV at 6.4 keV. To examine this width with the best possible energy resolution, we created spectra only from the single-pixel (pattern=0) events. The fits to the spectra from the pn, MOS1, and MOS2 yield the line widths of 56^{+25}_{-31} , 100^{+59}_{-49} , and 59^{+62}_{-59} eV, respectively. Thus, the line profile in each detector favors $\sigma \sim 60$ eV independently. If we assume that this line width originates from gas with Keplerian velocity, the line-emitting region is estimated to be located at approximately 10^4 Schwarzschild radii. However, the observed line width could instead be a result of a blend of ionization states. Then, the iron line emitter could be located at radii larger than $\sim 10^4$ Schwarzschild radii.

Variability is also a useful tool in constraining the location of the line-emitting region. Lack of short-term variability during the *XMM-Newton* observation (the duration is $\sim 5 \times 10^4$ s) implies that the region is separated from the nucleus by $\gtrsim 10^{-4}$ pc in order to smear out the variability of the continuum. On the other hand, long-term variability of the iron line was observed. From the long-term variability, the region is inferred to be located within $\lesssim 1$ pc from the nucleus. The inferred distance suggests that the region reprocessing the iron line is the outer part of the accretion disk and/or the torus.

6.4. Short-Term Variability

It should be noted that we detected rapid and rather high amplitude variability (Figure 3); such variability is rarely detected among Seyfert 2 galaxies (e.g., Turner et al. 1997). Turner et al. (1997) analyzed *ASCA* data from 25 Seyfert 2 galaxies (including eight narrow emission line galaxies). Of these, only five objects were bright enough to investigate short-term variability, and three of the five objects¹² were found to lie within the trend from a Seyfert 1 sample (Nandra et al. 1997). To compare our NGC 6300 result with their Seyfert 1 and 2 samples, we quantified the variability in the same manner as they do using the normalized excess variance (σ_{RMS}^2) for the light curve binned at 128 s in the 0.5–10 keV band. The value of $\sigma_{\text{RMS}}^2 = 0.107 \pm 0.009$ from the pn and the 2–10 keV intrinsic luminosity of 1.2×10^{42} ergs s $^{-1}$ are consistent with the trend from their Seyfert 1 sample. Awaki et al.

¹²All three are narrow emission line galaxies, and the only Seyfert 2 galaxy (NGC 1068) that was bright enough to investigate short-term variability did not show significant short-term variability.

(2004) provide more discussion on variability properties of NGC 6300 in comparison with other Seyfert galaxies and estimates of central mass using the power density spectrum, as well as other methods.

6.5. On the Optical Reddening

The soft X-ray spectrum suggests that the intrinsic absorption of this system is less than $N_H = 1-2 \times 10^{21} \text{ cm}^{-2}$ (§5.2.3); however, the optical spectrum from NGC 6300 is highly reddened (e.g., Lumsden, Alexander, & Hough 2004). Based on the fact that the emission lines are polarized to the same degree as the continuum (e.g., Lumsden et al. 2004) and on the presence of a prominent dust-lane that may lie in the line of sight to the nucleus (e.g., Maddox et al. in prep.), it seems plausible that the polarization and reddening originate in the host galaxy. If so, there should be gas associated with the dust, and that gas should attenuate the X-ray spectrum.

We can estimate the intrinsic column as follows. Lumsden et al. (2004) report an observed Balmer decrement ($H\alpha/H\beta$) of 8.7. We note that this value is uncertain. The optical nucleus of NGC 6300 is weak, and any observation is likely to contain a significant amount of light from the host galaxy; the presence of stellar spectral features (e.g., Na I D) can be seen in the spectrum published by Lumsden et al. (2004). Thus, the nuclear continuum and the $H\beta$ emission line may be difficult to distinguish from the galaxy light and stellar $H\beta$ absorption line without careful template subtraction (e.g., Halpern & Filippenko 1994). Regardless, using the Cardelli, Clayton, and Mathis (1989) reddening law, we infer that the Balmer decrement would be 7.9 after accounting for the reddening in our Galaxy [$E(B-V) = 0.097$; Schlegel et al. 1998]. If the intrinsic $H\alpha/H\beta$ ratio is 3.1 (Halpern & Steiner 1983), a Balmer decrement of 7.9 corresponds to $E(B-V)$ of 0.89. This corresponds to $N_H \approx 3.7 \times 10^{21} \text{ cm}^{-2}$, if the dust-to-gas ratio in NGC 6300 is the same as it is in our Galaxy (Heiles, Kulkarni & Stark 1981).

The deduced column density of the absorbing gas is much lower than that deduced from the hard X-ray spectral shape, as Maiolino et al. (2001) found a quite low $E(B-V)/N_H$ among Seyfert galaxies. However, our estimate of $E(B-V)$ is based on extinction for narrow lines; hence, it should be rather distant from the nucleus. Therefore, the dust may not be cospatial with the gas absorbing the hard X-ray, as we discussed in §5.2.2 regarding this object, and as Weingartner & Murray (2002) suggested in general.

On the other hand, the absorption of the soft X-ray emission could cospatially exist with the dust optical extinction because soft X-ray emissions from photoionized plasma are

reported to be associated with the (extended) narrow-line region (e.g., Sako et al. 2000; Yang, Wilson & Ferruitet 2001). We fitted the 0.2–1.6 keV spectra with a model including intrinsic absorption while N_{H} was fixed at the value deduced above. The fits with a power-law model were not rejected statistically ($\chi^2_{\nu} = 1.17$ and 0.84 for 34 dof for BGD1 and BGD2, respectively). However, the power-law index obtained is quite steep ($\Gamma = 4.8 \pm 0.2$ and 4.3 ± 0.4 for BGD1 and BGD2, respectively), suggesting that this model is unphysical by contrast with an origin of the power-law as energy-independent electron scattering of the primary continuum. Thus, if the soft X-ray emission is seen through the same medium as optical narrow emission-lines, the dust condition in the medium may be different from that in our Galaxy; for example, the deduced smaller $N_{\text{H}}/\text{E(B-V)}$ suggests that NGC 6300 may have a larger dust-to-gas-ratio and/or smaller grain size.

7. Summary

We investigated the nucleus of NGC 6300 using the results from a half-day observation by *XMM-Newton*. The X-ray spectrum of the nucleus consists of a heavily absorbed hard component dominating in the 3–10 keV band and a soft component seen in the 0.2–2 keV band. In the hard band, the spectrum is well fitted by a power-law model with a photon index of 1.83 ± 0.08 attenuated by a Compton-thin absorber ($N_{\text{H}} \simeq 2.2 \times 10^{23} \text{ cm}^{-2}$). A narrow iron line is detected at $6.43^{+0.01}_{-0.02}$ keV with $\text{EW} \sim 150$ eV; the line velocity width is marginally resolved to be $\sigma \sim 60$ eV. The observed properties of the iron line suggest that the origin is the outer part of the accretion disk and/or the putative torus. The decline of both the iron line and the reflection continuum fluxes on a time scale of years is observed, which implies that the nucleus has experienced an overall long-term trend of decreasing intensity on the same timescale. The Compton-thin absorber attenuating the hard X-ray continuum is more compact than a few hundred parsecs. Soft X-ray emission is likely to be electron-scattered light from a spatially extended region, and emission from a photoionized plasma is also likely to contribute to it.

This work is based on the observation obtained with *XMM-Newton*, an ESA science mission with instruments and contributions directly funded by ESA Member States and NASA. We acknowledge the great efforts of all of the members of the *XMM-Newton* team. We thank Dr. Guainazzi for providing a complete set of parameters for his *Beppo-SAX* spectral model and an anonymous referee for useful comments. K.M.L. acknowledges useful conversations with Rick Pogge regarding nuclear reddening. This work is partially supported by the *XMM-Newton* AO1 grant (NAG 5-9991).

REFERENCES

Awaki, A., Murakami, H., Leighly, K. M., Matsumoto, C., Hayashida, K., & Grupe, D. 2004, submitted to ApJ.

Awaki, H. 1991, Ph. D. thesis, University of Nagoya

Cardelli, J. A., Clayton, G. C., & Mathis, J. S. 1989, ApJ, 345, 245

den Herder, J. W., et al 2001, A&A, 365, L7

Dickey, J. M. & Lockman, F. J. 1990, ARA&A, 28, 215

Fabbiano, G., Kim, D.-W., Trinchieri, G. 1992, ApJS, 80, 531

Ghizzardi S. 2001; XMM-SOC-CAL-TN-0022

Guainazzi, M. 2002, MNRAS, 329, L13

Halpern, J. P., & Fillipenko, A. V. 1984, ApJ, 285, L475

Halpern, J. P., & Steiner, J. E. 1983, ApJ, 269, 37

Heiles, C., Kulkarni, S., & Stark, A. A. 1981, ApJ, 247, L73

Jansen, F., et al. 2001, A&A 365, L1

Leighly, K. M., Halpern, J. P., Awaki, H., Cappi, M., Ueno, S., & Siebert, J. 1999, ApJ, 522, L209

Lumsden, S. L., Alexander, D. M. & Hough, J. H. 2004, MNRAS, 348, 1451

Maddox, L. A., Leighly, K. M., Nava, A., Matsumoto, C., & Grupe, D. 2002, BAAS, 34, 1183

Maiolino, R., Marconi, A., Salvati, M., Risaliti, G., Severgnini, P., Oliva, E., La Franca, F., & Vanzi, L. 2001, A&A, 365, 28

Mathewson D. S. & Ford V. L. 1996, ApJS, 107, 97

Matt, G., Guainazzi, M., & Maiolino, R. 2003, MNRAS, 342, 422

Matt, G., Perola, G. C., & Piro, L. 1991, A&A, 247, 25

Nandra, K., George, I. M., Mushotzky, R. F., Turner, T. J., & Yaqoob, T. 1997, ApJ, 477, 602

Nava, A., Maddox, L. A., Matsumoto, C., Leighly, K. M., & Grupe, D. 2003, Proc. of “The Eighth Texas-Mexico Conference on Astrophysics: Energetics of Cosmic Plasmas”, ed. M. Reyes-Ruiz, E. Vázquez-Semadeni, RevMexAA SC, 18, 72

Sako, M., Kahn, S. K., Paerels, F., & Liedahl, D. A. 2000, ApJ, 543, L115

Sambruna, R. M., Netzer, H., Kaspi, S., Brandt, W. N., Chartas, G., Garmire, G. P., Nousek, J. A., & Weaver, K. A. 2001, ApJ, 546, L13

Schlegel, D. J., Finkbeiner, D. P., & Davis, M. 1998, ApJ, 500, 525

Strüder L., et al. 2001, A&A, 365, L18

Turner M. J. L., et al. 2001, A&A, 365, L27

Turner, T. J., George, I. M., Nandra, K., & Mushotzky, R. F. 1997, ApJS, 113, 23

Weingartner, J. C. & Murray, N. 2002, ApJ, 580, 88

Yang Y., Wilson A. S. & Ferruit P. 2001, ApJ, 563, 124

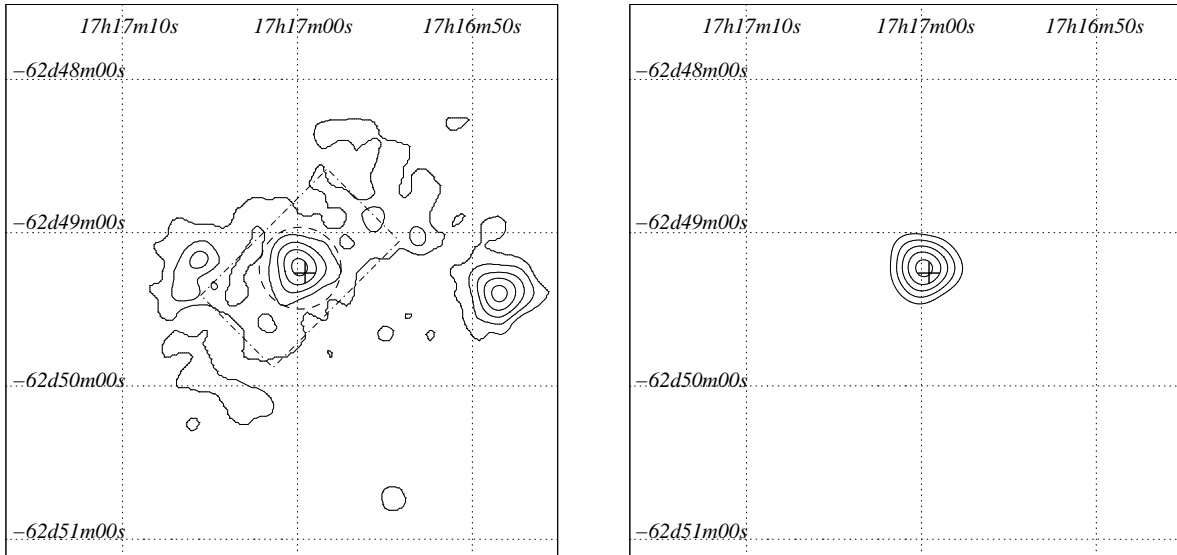


Fig. 1.— EPIC images of NGC 6300 in the energy bands of 0.2–2 keV (left) and 2–10 keV (right). Since the source falls near the chip gap of the pn, only the MOS data are used to make these plots. The images are smoothed with $\sigma = 3.2''$. The contours are drawn such that each step corresponds to a factor of 1.8 difference, and the first and last contours differ by an order of magnitude. In the left figure, the extraction region ($r < 16''$) for the soft spectrum is shown by the dashed line. A set of soft background spectra (BGD2; see §5.2) was collected from the rectangular region enclosed by the dot-dashed line excluding the $r < 20''$ from the nucleus. The radio core position is marked by the cross.

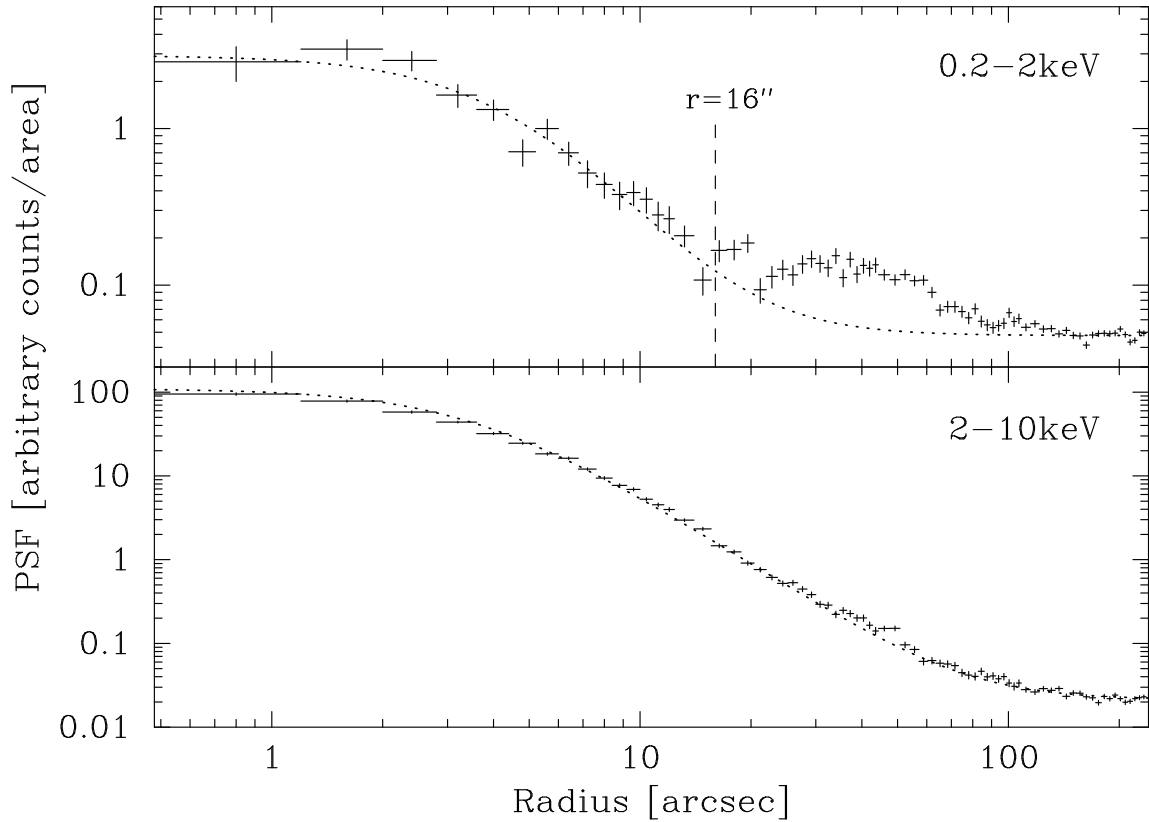


Fig. 2.— Radial profiles of the nucleus from the MOS detectors in the soft band (top) and the hard band (bottom). The PSF models of King profiles given by Ghizzardi (2001) are shown with constant offset which represents the background. The hard radial profile follows well along the PSF model; however, the soft one shows an excess for $r \sim 20\text{--}60''$ owing to the emission from the host galaxy. A radius of $16''$ is adopted for extraction of the soft spectrum.

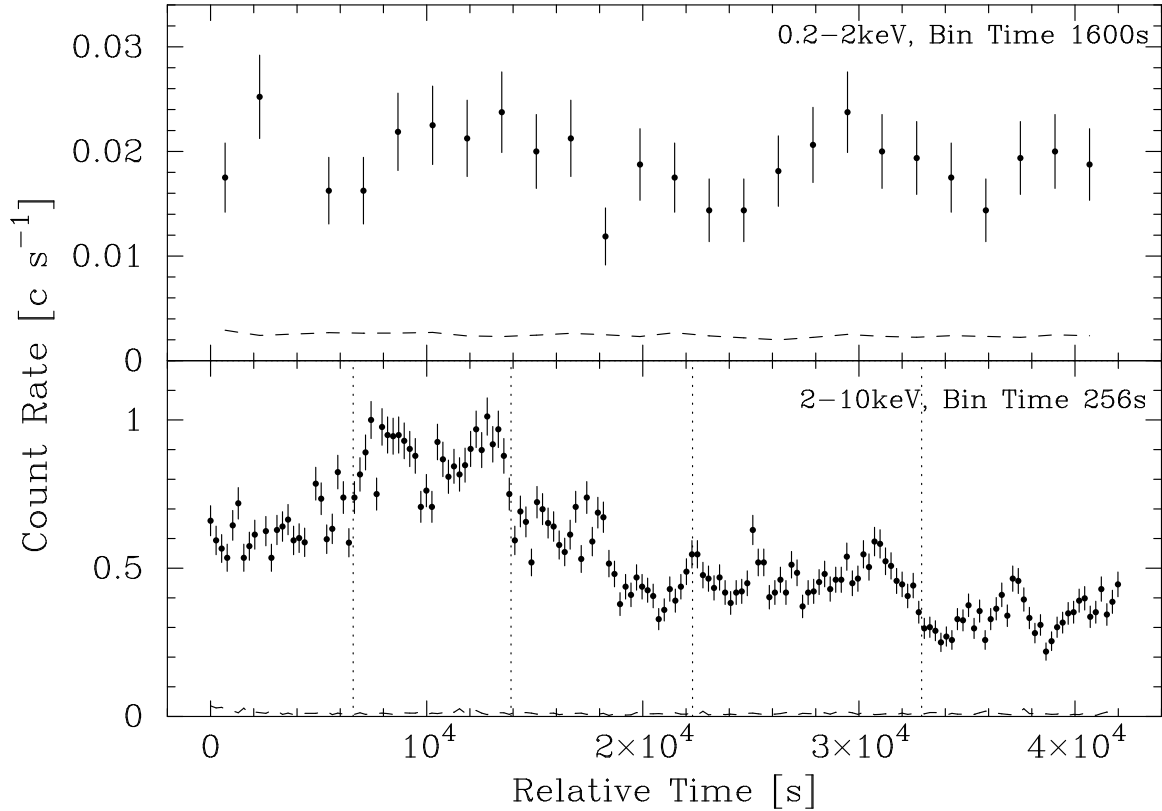


Fig. 3.— The pn light curve of NGC 6300 in the energy bands of 0.2–2 keV (top) and 2–10 keV band (bottom). The soft and hard photons were collected from the region centered at the X-ray peak within the radii of 16'' and 60'', respectively. The horizontal dashed lines show background levels (from the BGD1 region). The vertical dotted lines in the bottom panel are shown for the time-resolved spectral analyses in §5.1.

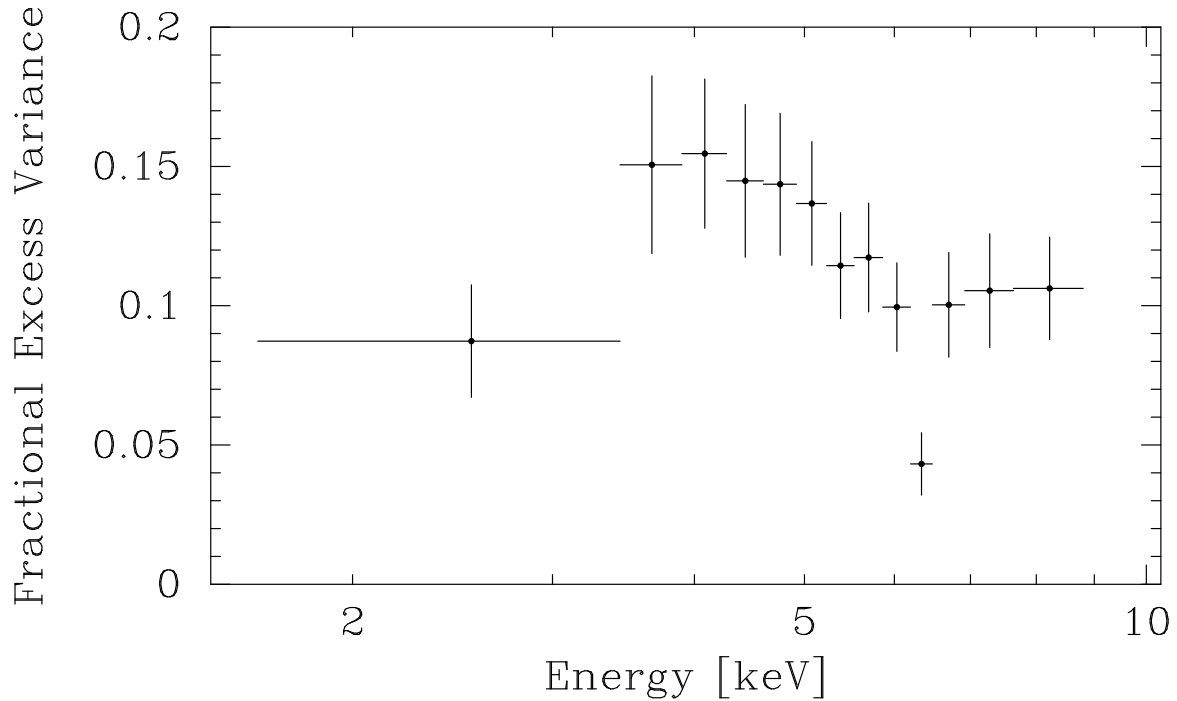


Fig. 4.— Poisson-noise-subtracted variance normalized by the mean count rate. Energy-resolved light curves from the pn and MOS data are binned at 384 s. Energy bands were chosen so that the same number of photons was included in each light curve. The reduced variability around 6.4 keV implies a less-variable iron line.

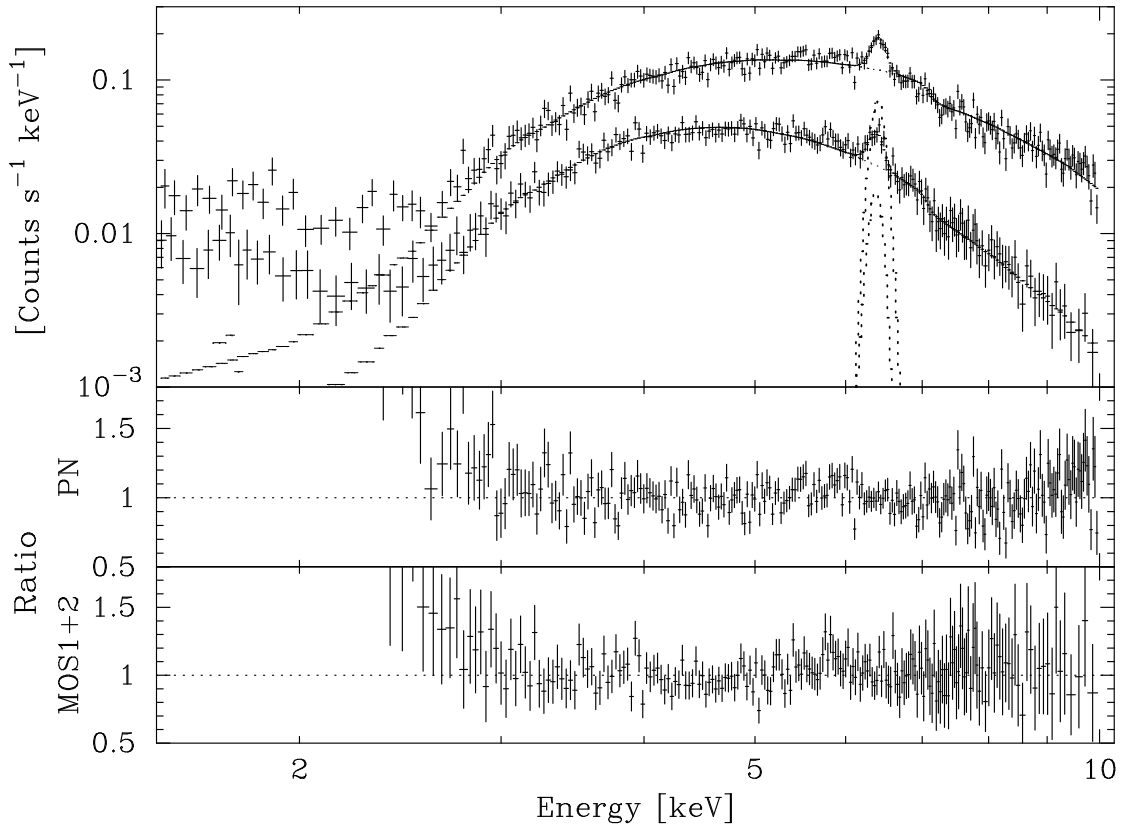


Fig. 5.— Hard X-ray spectra of the nucleus. Top: pn and MOS1+2 data in the hard X-ray band with the best-fit model (Compton-thin absorbed power-law plus a Gaussian line). The model was fitted only in the 3–10 keV band and then was extrapolated for the plots. The middle and bottom panels show the ratio of the data to the best-fit model for the pn and MOS1+2, respectively. These show that the soft component emerges below ~ 2.5 keV.

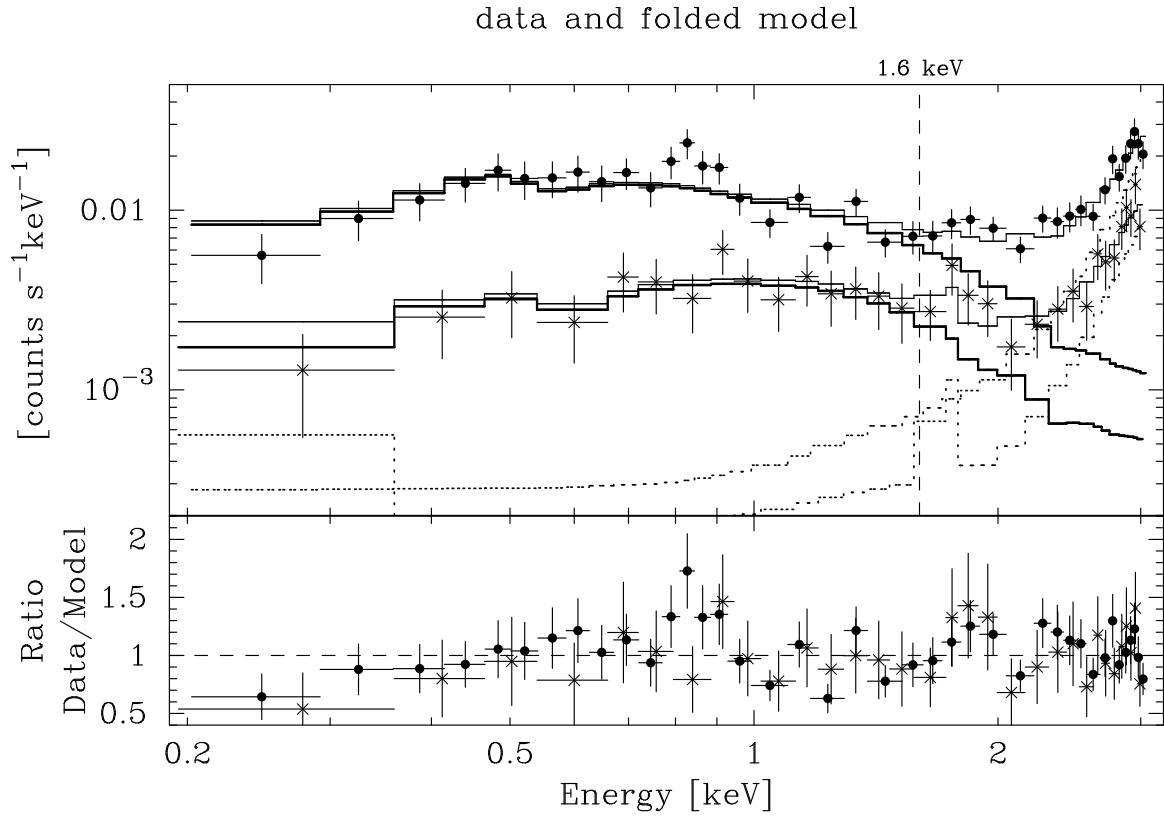


Fig. 6.— Soft X-ray spectra of the nucleus. The data from the pn and the MOS are marked by filled circles and crosses, respectively. The soft emission was modeled with the Galactic-absorbed power-law (thick solid lines). BGD1 is used for this figure. The fit was performed only in the 0.2–1.6 keV band, to avoid contamination from the hard X-ray emission (shown by the dotted lines for reference; the model parameters were taken from Table 3). The bottom panel shows the ratio of the data to the model including the hard components. The overall spectrum is reproduced by the model, but there are hints of emission line-like features around 0.8 and 1.9 keV.

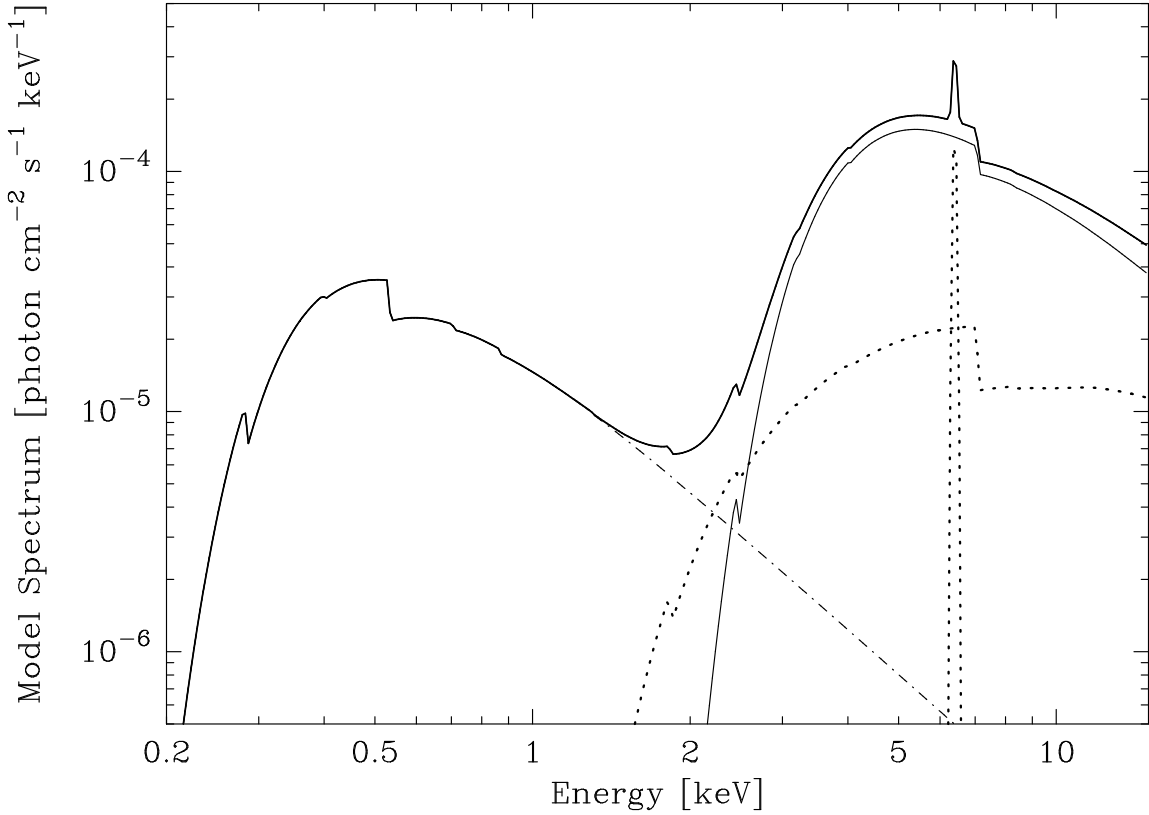


Fig. 7.— Final inferred model spectrum in the whole band. The parameters are listed in Table 3. The thick solid line represents total observed flux. The thin solid line shows the hard power-law attenuated by the intrinsic absorption of $N_{\text{H}hard}$. The dotted lines represent the reprocessed emissions (reflection continuum and an iron emission line) attenuated by another absorber of $N_{\text{H}repr}$. Although the soft X-ray spectrum is simply modeled by a power-law (dot-dashed line), the presence of some emission line-like features is suggested (see Figure 6 and §6.1). Thus, the soft emission could be emission from a photoionized plasma imprinted by many emission lines and radiative recombination edges.

Table 1. Results from the fits in the 3–10 keV band

Data	N_{H}^{a}	Γ	$F_{2-10\text{keV}}^{\text{b}}$	E_{Fe} [keV]	σ_{Fe} [eV]	F_{Fe}^{c}	χ^2/dof
pn	$2.14_{-0.10}^{+0.10}$	$1.85_{-0.09}^{+0.09}$	$2.16_{-0.12}^{+0.11}$	$6.43_{-0.02}^{+0.01}$	49_{-32}^{+24}	$3.1_{-0.4}^{+0.5}$	291.7/231
M1	$2.03_{-0.16}^{+0.17}$	$1.60_{-0.18}^{+0.18}$	$2.05_{-0.16}^{+0.18}$	$6.42_{-0.02}^{+0.03}$	62_{-45}^{+37}	$3.5_{-0.9}^{+0.9}$	164.7/153
M2	$2.08_{-0.17}^{+0.17}$	$1.81_{-0.18}^{+0.19}$	$2.05_{-0.17}^{+0.20}$	$6.40_{-0.03}^{+0.02}$	$55(< 38)$	$3.0_{-0.7}^{+0.9}$	151.5/152
pn&MOS	$2.15_{-0.09}^{+0.08}$	$1.83_{-0.08}^{+0.08}$	$2.16_{-0.10}^{+0.10}$	$6.43_{-0.02}^{+0.01}$	55_{-21}^{+19}	$3.2_{-0.4}^{+0.4}$	423.5/420

^aHydrogen equivalent column density of intrinsic absorption in the unit of 10^{23} cm $^{-2}$.

^bAbsorption-corrected power-law flux in the 2–10 keV band. The units are 10^{-11} erg cm $^{-2}$ s $^{-1}$.

^cIron line flux in the units of 10^{-5} photon cm $^{-2}$ s $^{-1}$.

Note. — Here we assumed that the line is also attenuated by the same intrinsic absorption as the continuum; if the line is observed without intrinsic absorption, the line intensity becomes weaker (transmission efficiency of $N_{\text{H}} \sim 2.2 \times 10^{23}$ cm $^{-2}$ absorption is 69% at 6.4 keV)

Table 2. The soft X-ray band fits with a power-law (PL) or an optically-thin thermal model (RS)

Model	BGD	Intrinsic Abs. ^a	Γ or kT [keV]	$F_{0.2-2\text{keV}}^b$	Z^c	χ^2/dof
PL	BGD1	...	$2.00^{+0.16}_{-0.18}$	7.2 (3.7)	...	32.36/35
	BGD2	...	$1.72^{+0.26}_{-0.28}$	4.9 (2.8)	...	21.80/35
	BGD1	$0.9^{+1.1}_{-0.8}$	$2.8^{+0.8}_{-0.7}$	15. (3.5)	...	28.47/34
	BGD2	0.5 (<1.5)	$2.1^{+1.2}_{-0.9}$	6.7 (2.7)	...	21.34/34
RS	BGD1	...	$1.2^{+0.4}_{-0.2}$	6.6 (3.6)	0 (<0.01)	29.99/34
	BGD2	...	$2.1^{+3.2}_{-0.8}$	4.6 (2.8)	0 (<0.14)	21.57/34
	BGD1	0.2 (<0.8)	$1.0^{+0.5}_{-0.4}$	7.5 (3.5)	0 (<0.01)	29.34/33
	BGD2	0.05 (<1.0)	$2.0^{+3.3}_{-1.2}$	4.7 (2.7)	0 (<0.12)	21.56/33

^aHydrogen equivalent column density of intrinsic absorption in the units of 10^{21} cm^{-2} .

^bFlux in the 0.2–2 keV band in units of $10^{-14} \text{ erg cm}^{-2} \text{ s}^{-1}$. The fluxes are corrected for absorption; the values in parentheses are absorption-uncorrected fluxes.

^cInferred abundance in units of solar.

Table 3. The best-fit model in the whole energy band

Γ	Norm _{soft} ^a $\times 10^{-5}$	$N_{\text{H}}^{\text{hard}}$ ^b $[10^{23} \text{ cm}^{-2}]$	Norm _{hard} ^a $\times 10^{-3}$	$N_{\text{H}}^{\text{repr}}$ ^c $[10^{23} \text{ cm}^{-2}]$	R^{d} $[\Omega/2\pi]$	E_{Fe} [keV]	σ_{Fe} [eV]	F_{Fe} [photon $\text{cm}^{-2} \text{ s}^{-1}$]	χ^2/dof
1.94 ± 0.09	$1.83^{+0.14}_{-0.13}$	$2.4^{+0.1}_{-0.2}$	$7.7^{+1.4}_{-1.2}$	$0.4^{+0.3}_{-0.2}$	$1.1^{+1.2}_{-0.6}$	$6.42^{+0.02}_{-0.01}$	49^{+21}_{-28}	$(2.4 \pm 0.3) \times 10^{-5}$	438.73/475

^aPower-law normalization at 1 keV in the rest frame. The units are photon $\text{cm}^{-2} \text{ s}^{-1}$.

^bColumn density of the absorption for the hard power-law emission.

^cColumn density of the absorption for the reprocessed components (reflection and a fluorescent iron line).

^dReflection strength. The incident emission is assumed to be same as the observed hard power-law emission. The other parameters were taken from Leighly et al. (1999; inclination angle of 77° from the normal, abundances of 0.66 solar, power-law cut-off of 500 keV), and fixed at those values while fitting.

Table 4. Flux change in the hard X-ray band during 4 years

Observation		Total ^a [erg cm ⁻² s ⁻¹]	Reflection ^b [10 ⁻¹² erg cm ⁻² s ⁻¹]	Iron-Line ^b [10 ⁻⁵ photon cm ⁻² s ⁻¹]	Iron EW ^c [eV]
<i>RXTE</i>	1997 Feb	6.4×10^{-12}	6.4	$4.7^{+1.2,+1.2e}_{-1.0,-1.2}$	$470^{+120,+200e}_{-100,-150}$
<i>Beppo-SAX</i>	1999 Aug	1.3×10^{-11}	$6.5^{+4.0}_{-2.6} d$	3.6 ± 1.7	$310^{+190}_{-240} f$
<i>XMM-Newton</i>	2001 Mar	8.6×10^{-12}	$1.3^{+1.4}_{-0.7} d$	2.4 ± 0.3	$990^{+1030}_{-560} g$

^aObserved fluxes in the 2–10 keV band.

^bThe fluxes were corrected for absorption. The reflection fluxes are in the 2–10 keV band.

^cIron-line EW with respect to the reflection component.

^dThe flux error is estimated by propagating the uncertainties in R . In principle, this is also subject to the uncertainty in the absorption.

^eThe first one is the statistical error; the second one is an estimate of the systematic error obtained by changing the normalization of the background.

^fThe EW error is estimated assuming that the errors of R and the iron-line intensity are independent.

^gSince the line flux is constrained much better than the reflection flux, the EW error is estimated by scaling the error in R .

Note. — The *XMM-Newton* parameters are obtained using spectral model in Table 3. The parameters for *RXTE* and *Beppo-SAX* are from Table 1 “Compton Reflection Model” of Leighly et al. (1999) and Table 1 “Model 3” of Guainazzi (2002), respectively. The *Beppo-SAX* model assumed that both the reflection and the iron-line are attenuated by the absorption same as the power-law emission ($N_{\text{H}} = 2.2 \times 10^{23} \text{ cm}^{-2}$). Assuming that the iron-line is not attenuated by the absorption, the flux is about 30% weaker. In our *XMM-Newton* fit, we assumed that the reprocessed emission is attenuated by an absorber different than that for the nuclear power-law emission. The absorption column density of the reprocessed emission is $4 \times 10^{22} \text{ cm}^{-2}$, and its attenuation magnitude is about 7% at 6.4 keV.